DOI:
10.1039/c8cp00543e

Document Version
Peer reviewed version

Journal Name

ARTICLE

PRODAN differentially influences its local environment

Received 00th January 20xx,
Accepted 00th January 20xx

DOI: 10.1039/x0xx00000x

www.rsc.org/

Adam Suhaj,[a] Alix Le Marois[b], David J. Williamson[c], Klaus Suhling[b], Christian D. Lorenz[b] and Dylan M. Owen[a]

Environmentally-sensitive membrane dyes have been extensively used to study the different liquid phases, (liquid-ordered (Lo) and liquid-disordered (Ld)) of the heterogenous cellular membrane. However, it is not yet well understood how these dyes affect membranes properties upon and post insertion. Using a combination of molecular dynamics (MD) simulations and fluorescence microscopy, we study the effect of PRODAN insertion upon its local environment. We firstly present the results of the MD simulations of PRODAN interacting with lipid bilayers of various compositions, specifically the resultant hydration and lipid order of the system. Experimentally, the lipid order of Lo and Ld vesicles containing various concentrations of PRODAN are inferred from their Generalised Polarisation (GP) values, calculated using their fluorescence spectra. We then apply the methodology to a more complex biological system, the HeLa cell line. For both systems, the presence of PRODAN influences its local environment differently between the Lo and Ld phases. In the simulated systems, the presence of PRODAN lowers the lipid order in the Ld phase and increases the order in Lo phase, whilst experimental data demonstrates that even a small increase in PRODAN concentration significantly lowers the order of both phases. We suggest this discrepancy may be ascribed to the differing localisations of the dye molecules within the bilayer, and their effect on the hydration of adjacent lipids.

Introduction

The plasma membrane is an important cell structure responsible for many processes such as cell signalling[1] and ion transportation.[2] For most of their history, the organisational or regulatory role of lipids within the cell membrane was not fully appreciated. However, the discovery that several membrane proteins are attached to the membrane through a GPI lipid 'anchor'[3] suggested that different membrane proteins exhibit various affinities for different lipids. This led to the proposed existence of lipid rafts[4] within the cell membrane. The raft hypothesis suggested that the membrane is a complex system of distinct and separated membrane phases; the liquid ordered (Lo) and the liquid disordered (Ld) phase. More recently, the idea has been updated further with evidence that there exists a dynamic raft-based heterogeneity at the nanoscale within the membrane.[5,6] This new model had an important and far-reaching impact on the field and is now thought to be responsible for a variety of processes, most importantly protein clustering[7] and signal transduction[1,8,9]. To study these distinct lipid phases, environmentally sensitive (ES) probes have been commonly used for many decades[10–16]. Due to the intrinsic differences between Lo and Ld phases, these probes change their spectroscopic properties dependent upon environmental factors, such as hydration or viscosity[13,17]. When environmentally sensitive dyes such as PRODAN are excited, the dipole moment of the dye changes[18]. If these dyes exist in a polar environment, they undergo dipolar relaxation where some of the energy of their excited state is lost through the rearrangement of the surrounding polar molecules, owing to the change in the dyes' dipole moments[19].

Despite their long and widespread use, the effect that the dye exerts on the membrane itself, in terms of biophysical and spectroscopic properties, has been comparatively understudied although some experimental studies on the effect of the dye on the bending elasticity[20] and miscibility transition[21] have been performed. Whilst some molecular dynamics (MD) studies have been performed regarding the position and electron densities of ES dyes and water in lipid bilayers[17,22], to the best of our knowledge, no studies using MD have investigated their effect on the surrounding lipids at the nanoscale, in two distinct lipid phases.

Here, we investigate the incorporation of PRODAN molecules into Lo and Ld lipid bilayers and the effect that the dye molecules exert both on the deuterium lipid order parameter and the hydration of the surrounding lipids upon PRODAN excitation. For this, we use a combination of MD simulations and fluorescence microscopy studies of giant unilamellar vesicles (GUVs) of the same composition. Whilst PRODAN has fallen out of favour as an environmentally sensitive dye and has been replaced by more modern and

[a] Department of Physics and Randall Division of Cell and Molecular Biophysics, King's College London, London, UK.
[b] Department of Physics, King's College London, London, UK.
[c] Randall Division of Cell and Molecular Biophysics, King's College London, London, UK.

Electronic Supplementary Information (ESI) available: [details of any supplementary information available should be included here]. See DOI: 10.1039/x0xx00000x

robust dyes such as Laurdan (6-lauryl-2-dimethylamino-napthalene) [14] or di-4-ANEPPDHQ[23], it was chosen as the molecule of interest due to its relative structural simplicity. It also represents a great stepping stone towards studies of the aforementioned complex dyes, owing to their chemical similarities and current lack of MD models of these dyes. Lastly, we corroborate our findings with live cell fluorescence imaging of HeLa cells stained by PRODAN.

Experimental

Materials

1,2-Dioleoyl-sn-glycero-3-phosphocholine (DOPC) and 1,2-dipalmitoyl-sn-glycero-3-phosphocholine (DPPC) were purchased from Avanti Lipids in powder form. Water free chloroform used for dissolving lipids was obtained from Sigma-Aldrich. 6-Propionyl-2-dimethylaminoaphthalene (PRODAN) was purchased from AnaSpec in powder form. Dulbecco's Modified Eagle Medium (DMEM), Fetal Bovine Serum (FBS) and L-Glutamine were purchased from ThermoScientific.

Vesicles preparation and imaging

GUVs were prepared using the gentle hydration method[24]. Homogeneous DOPC vesicles were first prepared by dissolving DOPC lipids in chloroform at a concentration of 10 mM. Ordered phase vesicles were prepared in similar fashion, in a chloroform solution of 70% DPPC + 30% Cholesterol (7 mM DPPC / 3 mM cholesterol). PRODAN dissolved in DMSO was added to the solution in at the desired concentration: 39, 100, 200, 300, 500 and 800 µM, to achieve a wide range of dye:lipid ratios (1:256/1:284, 1:100, 1:50, 1:33.3, 1:20 and 1:12.5 respectively). Organic solvents in the solutions were left to evaporate over the course of several hours until dry lipid films with PRODAN formed. The lipid films were subsequently hydrated overnight in distilled water at room temperature (RT) for DOPC vesicles, and in a 49°C water bath for DPPC:Chol vesicles.

For vesicle imaging, 100 µL of the stock solution was diluted in 400 µL of distilled water. The diluted solutions of different PRODAN concentrations were pipetted into an 8 well plate and left at 4°C overnight to allow the vesicles to settle on the bottom of the plate. The vesicles were imaged using Nikon Eclipse Ti-E Inverted confocal microscope with a 100x oil immersion objective and a 405 nm diode excitation laser. A 32-channel Spectral Detector was used to measure the spectra of the vesicles at 405 and 600 nm.

Fluorescence lifetime measurements of PRODAN in vesicles were carried out on a custom-built fluorescence lifetime imaging (FLIM) system. The sample was excited using a picosecond-pulsed 375 nm diode laser (Horiba DDL series) with a repetition rate of 25 MHz. The laser beam was coupled into a TCS SP2 microscope (Leica) and focused onto the sample by a 63x, 1.2 NA water immersion objective lens (Leica). PRODAN fluorescence emission was collected through a 450 LP filter (ThorLabs) and detected by a cooled HPM 100-40 hybrid detector (Becker & Hickl). TCSPC was performed using a SPC-150 card (Becker & Hickl). Data was acquired in the 'Single' mode while scanning over individual vesicles, so that a single fluorescence decay was acquired for each vesicle. All imaging was performed at room temperature.

Cell preparation and imaging

To reach desirable confluency of HeLa cells for imaging, 5000 cells suspended in 300 µl of DMEM supplemented with 10% (v/v) FBS and 1x L-Glutamine were deposited in a well of an 8-well µ-Slide. The well slide was incubated overnight at 37°C in a humified 5% (v/v) CO_2 atmosphere. On the day of imaging, the supplemented culture medium was replaced with serum-free medium to prevent sequestering of the dye. The cells were stained with PRODAN dissolved in DMSO to achieve concentrations of: 3.7, 4.5, 5.3, 6.1 and 8.3 µM. To ensure that the dye had diffused through the sample, cells were incubated at 37°C in a humified 5% (v/v) CO_2 atmosphere for an hour post-staining

For cellular imaging, a 60x oil immersion objective and a 405 nm diode excitation laser was used. Two intensity channels, (425-475 nm) and (488-530 nm), were acquired and images used for spectral analysis. All imaging was carried out at RT. Controls were performed to check for cell auto-fluorescence contribution and excitation laser scattering. No significant contribution from these sources was observed (Fig. S1 and S2).

Image processing and analysis

To investigate the different lipid phases in the vesicles and cells, GP values were calculated according to the following equation[15]:

$$GP = \frac{I_{425-475} - I_{490-530}}{I_{425-475} + I_{490-530}} \quad (1)$$

where $I_{425\text{-}475}$ and $I_{490\text{-}530}$ are the intensities of the spectra between the stated wavelengths. GP values provide a measure of membrane lipid order and they are analogous to the classical fluorescence polarisation function. To counteract any contribution of fluorescence from free dye diffusing in water, regions of interests (ROIs) were manually selected to encompass the vesicles alone (or the desired cellular feature) and background intensity subtracted from the intensity of the ROIs. To ensure that there was no contribution of fluorescence from the dye in the water, fluorescence spectra of the imaging medium containing the same concentrations of PRODAN as was used in the cellular experiments were measured and compared to a spectrum of dye-free medium (Supplementary Fig. S2). Compared to a dye-free medium there is a negligible increase in background fluorescence from the dye. For vesicular data, the integral of their spectra between the necessary wavelengths was used for the intensities of the GP calculation. For cellular data, the intensity in the ordered (blue, 425-475 nm) and disordered (green, 490-530 nm) was used in Eq. 1, for each ROI. The subsequent analysis and data fitting was carried out in GraphPad Prism 7 software where the sum-of-squares F-tests were used to test for statistical significance. Fluorescence decay curves were analysed using Origin 2017 software.

Computational details

In the MD simulations, both excited- and ground-state PRODAN molecules were considered planar, since previous studies[13,25], and quantum mechanical (QM) calculations validate that the ground and first excited states exist in planar form. Both charge sets used, the ground and excited state in water, were first described by Nitschke et al.[22] where the excited state was vertically polarised, and these charge sets were used in the presented simulations. The forcefield used with PRODAN topology was the GROMOS9653a6 (G53a6) forcefield.[26,27] This forcefield explicitly considers the aromatic hydrogen atoms present, however it treats methyl and methylene groups as united atoms in PRODAN. The DOPC and DPPC molecules have been previously modelled by a G53a6 field modified by the Berger forcefield for lipid molecules.[28] Water molecules are described by the extended simple point charge model (SPC/E) which is a three-point model with an average polarisation included[29]. Cholesterol was also described by the G53a6 forcefield.

All MD simulations were performed with the GROMACS package version 5.1.3. The DOPC simulation box consisted of 512 DOPC molecules forming two leaflets, 2 ground state PRODAN molecules outside the leaflets and rest of the box was filled with water. The size of the box was 10.6262 x 10.6262 x 10.6797 nm^3. The DPPC-Chol simulation box consisted of 400 DPPC molecules with 168 Cholesterol molecules forming two leaflets, 2 ground state PRODAN molecules outside the leaflets and the rest of the box was filled with water. The size of the box was 13.0208 x 13. 0208 x 8.2937 nm^3. All equilibration and production simulations were performed with an integration step of 2 fs. The energy minimisation simulation was performed for 1000 steps for both systems, to allow the potential energy of the system reach its lowest value and resolve any close contacts within the systems that existed in the initial configuration. The constant volume (NVT) equilibration step brought the system to the desired simulation temperature of 300 K, by equilibrating the system consecutively at three increasing temperatures. Firstly, it was run at 100 K, then 200 K and lastly 300 K for 20 ps per stage. All NVT equilibrations were performed under the Nosé-Hoover thermostat.[30] Constant pressure (NPT) equilibration was also run to stabilise the pressure and the density of the system. It was run for 20 ps and brought the system to a pressure of 1.013 bar under semiisotropic conditions using a Parrinello-Rahman barostat.[31] In all simulations, periodic boundary conditions were employed and spherical cut-off radii of 1.4 nm were used for the van der Waals interactions, long-range Coulomb interactions were calculated using the particle mesh Ewald method[32], and the neighbour list was updated every 10 integration steps. All bonds in the simulations were constrained by the P-LINCS algorithm.[33] The main MD simulation of the insertion of ground state PRODAN for both bilayer systems was run for 100 ns. In the case of the DPPC:Chol system, an additional simulation was performed where the PRODAN molecules were initially inserted deep in the bilayer. The simulation was run for 20 ns. After a few nanoseconds of the simulation, the PRODAN molecules moved to the same location as in the main simulation (Fig. S3). Thus, we can say that the final position of the dye molecules in the main simulation is fully equilibrated. After the ground state PRODAN molecules became inserted in the bilayers the bilayers, their charge sets were switched for the first vertically excited charge set and the simulation was extended for 5 ns with the new charge set. This was performed to simulate the average fluorescence lifetime of PRODAN (4 - 5 ns).[12]

Results & Discussion

Simulation

The ordering of hydrocarbon chains in lipid bilayers is described by NMR deuterium order parameter (S_{CD})[34]:

$$S_{CD} = \frac{1}{2}\langle 3cos^2\theta - 1\rangle \quad (2)$$

Where θ is the angle between the carbon-deuterium (C-D) bond (in the case of our simulation the C-H) bond and the bilayer normal (z-axis). To investigate a possible change in lipid order with increasing distance from the PRODAN molecule, the order parameters were calculated for four distinct concentric annuli in the range of 4 - 20 Å, centred on the carbonyl oxygen of PRODAN. The lipids were assigned to the regions by calculating the distance between PRODAN's carbonyl oxygen and the phosphorus atom of the lipid.

DOPC bilayer simulation

Fig. 1A and 1B present the values of S_{CD} of the simulated DOPC hydrocarbon chains for different distances extending from PRODAN. In this simulated bilayer system, the S_{CD} values are lower for lipids closer to PRODAN, especially for those in the closest proximity. This can be seen in the sn-1 tail in which the chain order at carbon 9 decreases from ≈ 0.16 in the furthest region to ≈ 0.07 for the closest lipids. The largest difference is seen in the ten carbons closest to the headgroup, which corresponds to where PRODAN molecules are located in the DOPC system (Fig. 2A), suggesting that the presence of PRODAN is responsible for lower lipid order. Similarly, the hydration of the phosphate and choline group of the phospholipids in the same regions was investigated by determining the number of water molecules within their first hydration shell. In Figures 1C and 1D, the hydration probabilities (the probability that the first hydration shell of an atom will contain a specified number of water molecules) of the phosphate group for the ground and excited states, respectively, are shown. It appears that in the ground state the phosphate groups of the lipids in the closest region (4 - 7 Å) have an increased probability of high hydration whilst for the other three regions, very minor change is experienced. Universally, the hydration of all regions is increased post excitation, an effect which is most pronounced in the closest two regions to PRODAN. However, a contrasting pattern is evidenced in the hydration of the choline group, in which the 4-7 Å region is much more dehydrated (Fig. 1E) than the other three regions which are again similar to the case of

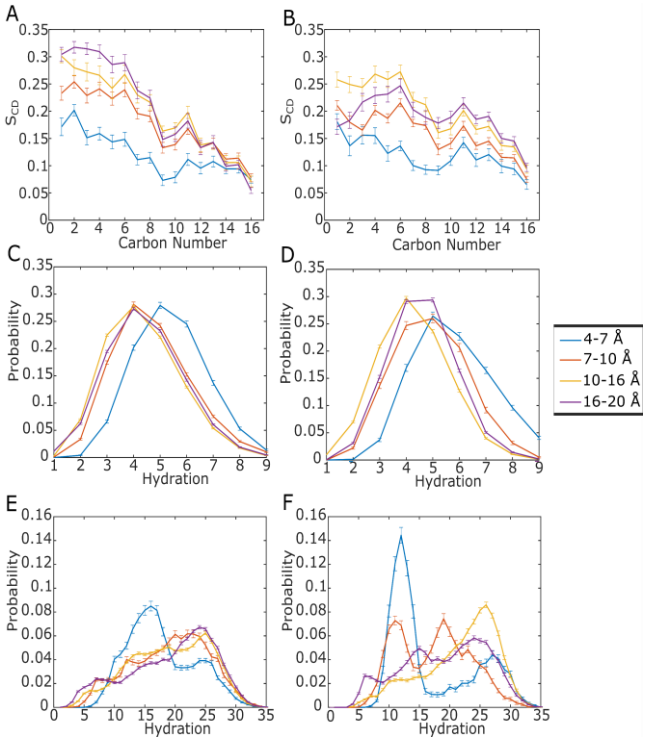

Figure 1: The deuterium order parameters of the DOPC sn-1 (A) and sn-2 (B) hydrocarbon tails are presented. Hydration probabilities of the first hydration shell of the DOPC phosphorus atom in the ground (C) and excited (D) state of PRODAN and of the DOPC nitrogen atom in the ground (E) and excited (F) states are also shown. Hydration probabilities were calculated from 4000 snapshots for the ground state and 2000 snapshots in the excited state.

PRODAN in its ground state. Post excitation, (Fig. 1F) the choline groups in the two innermost regions become significantly more dehydrated. These findings, in combination with the lipid order decrease, suggests that the presence of PRODAN decreases the order of the bilayer, possibly allowing more water molecules to penetrate deeper into the bilayer. This in turn causes an increase of hydration of the more deeply hidden phosphate group, whilst decreasing the hydration of the choline group located closer to the lipid-water interface.

Figure 2: The relative z-position of the centre-of-mass of PRODAN molecules with respect to the average z-position of the phosphate group in the DOPC (A) and DPPC (B) over time. The final resting positions of PRODAN molecules (thick magenta lines) in the DOPC (Ld) system (C) and the DPPC:Cholesterol (Lo) system (D). Water molecules are represented by thin cyan lines, cholesterol with bright green, nitrogen and phosphorus with blue and beige sphere respectively and the rest of the lipids with grey and light red lines.

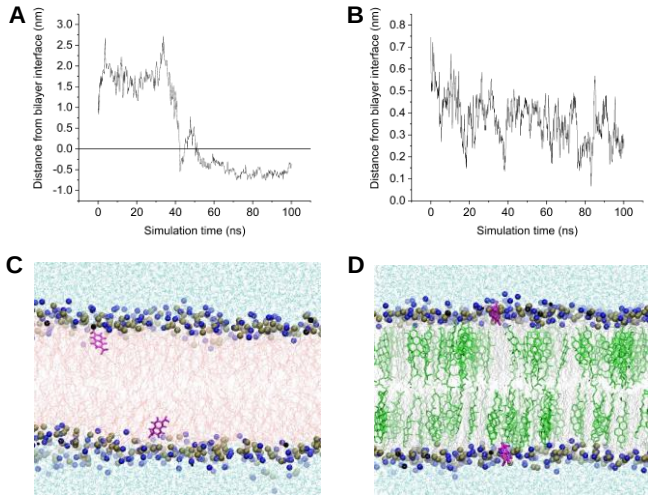

DPPC:Chol bilayer simulation

Results from MD simulations in the DPPC:Cholesterol system contrast with those of the DOPC configuration. Fig. 3A and 3B demonstrate that the hydrocarbon tails have on average a slightly higher lipid order closer to the carbonyl oxygen of PRODAN. The difference in order change between the two systems could be explained by the different penetration depths PRODAN molecules exhibit in the two systems. In the DPPC system, PRODAN remains in the polar headgroup region, directly above the phosphate group (Fig. 2B and 2D). The increase of S_{CD} is most pronounced in the carbon atoms closest to the lipid interface and thus the PRODAN molecule, while very little increase in order is seen in the carbon atoms further away from the bilayer interface. It is possible that the presence of PRODAN molecules in the headgroup region pushes the lipid headgroups away and restricts their movement, increasing their packing order. This kind of exertion of pressure on the nearby lipid headgroups could be responsible for the increase of order seen in the carbon atoms closest to the headgroup. However, further pressure and lipid motility studies must be performed to validate this hypothesis.

The study of hydration of the lipids in the DPPC:Chol bilayer also reveal an opposite behaviour to that of the DOPC bilayer. The hydration of the phosphate group in PRODAN's ground state is slightly lower in the closest lipids, whilst not significantly different in further regions (Fig. 3C). However, there is a substantial increase in the probability that the phosphate group will have 3 water molecules in its first hydration shell, but lower probability of higher hydration (Fig. 3D) for the DPPC:Chol bilayer. As shown in Figs. 3E and 3F, the choline groups closest to PRODAN experience a significant increase in their probability of high hydration when compared to other regions. Post excitation, a more complex pattern emerges, where the closest 4-7 Å region experiences an increased probability of low hydration.

These findings concerning bilayer hydration, in combination with the lipid order study suggests that the presence of PRODAN increases the order of carbon atoms closest to the bilayer interface, which as a result does not allow water molecules to penetrate deeper into the bilayer. It is suggested that as a result, the water molecules aggregate closer to the lipid-water interface around the choline group.

Investigation of cellular and vesicular GP values

As the simulated data suggested that the presence of PRODAN affects the order and hydration of the lipid bilayer, we next investigated the concentration of PRODAN required to achieve this disruption. It was hypothesised that with increased concentration of the dye, it was more likely that two or more PRODAN molecules within the bilayer would localise within the immediate vicinity of one another and this event could in turn disrupt the calculated GP values. Therefore, the effect of various PRODAN concentrations on the spectra of GUVs and live HeLa cells was investigated.

Figure 3: The deuterium order parameters of the DPPC sn-1 (A) and sn-2 (B) hydrocarbon tails are presented. Hydration probabilities of the first hydration shell of the DPPC phosphorus atom in the ground (C) and excited (D) state of PRODAN and of the DPPC nitrogen atom in the ground (E) and excited (F) states are also shown. Hydration probabilities were calculated from 4000 snapshots for the ground state and 2000 snapshots in the excited state.

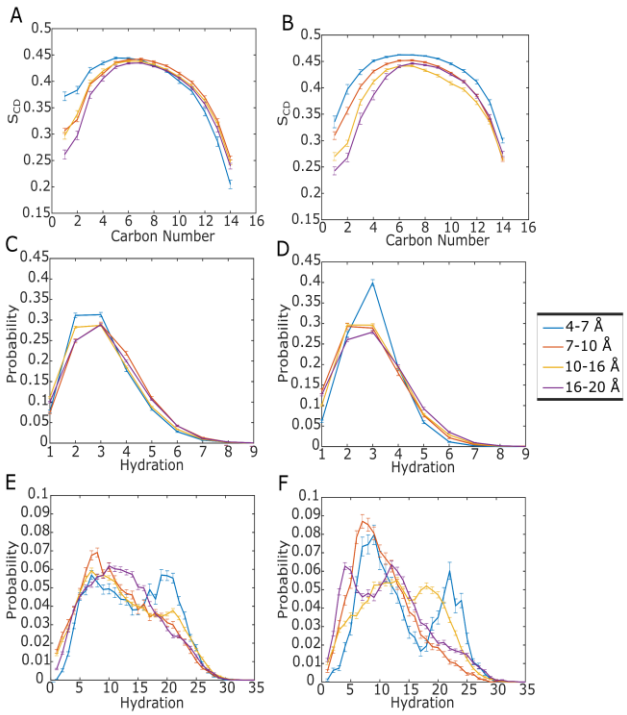

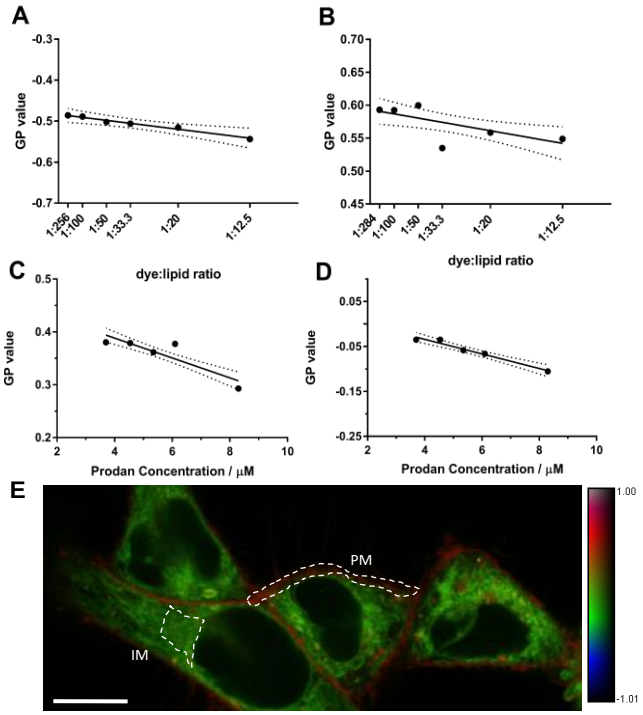

Figure 4: Calculated GP values for DOPC (A) and DPPC:Chol (B) vesicles with a linear regression (solid line) and the 95% confidence intervals (dotted line). GP values of the cellular membrane (C) and the intracellular system (D) for different concentrations, lines of best fit (solid) and 95% confidence intervals (dotted) are shown. (E) Merged rainbow RGB colour GP image and mean intensity of live HeLa cells. The image is in false colour and runs over the GP range indicated by the colour bar. White dotted regions show an example of ROIs used for GP analysis, where the plasma membrane (PM) is taken as analogous to Lo due to its high GP, and intracellular membrane (IM) analogous to the Ld phase due its relatively low GP. Scale bar, 10μM.

The Ld phase exhibits a very clear linear decrease in GP as the concentration of PRODAN increases (Fig. 4A). At a ratio of 1:256, the average GP is -0.48 ± 0.02 and it linearly decreases to -0.54 ± 0.01 at the 1:12.5 ratio ($P < 0.05$, N=15 for each ratio). This behaviour is to be expected and is consistent with the simulated system, which shows that PRODAN decreases lipid order and allows water molecules to penetrate deeper into the bilayer.

However, the Lo phase does not show the behaviour expected from the simulations. The GP value in the Lo vesicles is negatively correlated with the concentration of PRODAN from 0.59 ± 0.01 at 1:284 ratio to 0.55 ± 0.01 at the 1:12.5 ratio (Fig. 4B, $P = 0.01$, N=15 for every ratio). Whilst it was originally expected to increase as the presence of PRODAN increases, owing to the order of nearby lipids (Fig. 2A and 2B) the decrease in GP could be explained by the higher hydration of the choline group in those proximal lipids.

This discrepancy with the simulation data could be due to the diversity of location of PRODAN in the bilayers and by their different effect on the hydration of the surrounding lipids. When the concentration of PRODAN in the DPPC:Chol (Lo) bilayer increases, there may be an increased probability that the dye molecules become spatially proximal and create aggregate-like structures. However, as the MD simulations demonstrate, the dye molecules remain located at a distance significantly distal to the phosphate group of the lipids (Fig 2B) and closer to the bilayer-water interface. Even though PRODAN remains significantly closer to the bilayer-water interface in the DPPC:Chol bilayer, on average, there are water molecules within its first hydration shell (Table 1). However, the presence of PRODAN increases the hydration of the closest choline group (Fig. 3E) where the dye is localised. If the dye molecules are indeed very close to one another, the probability that they will be surrounded by highly hydrated choline groups is higher. Thus, the sensed GP value of the Lo phase could be lowered, despite the true positive effect that the dye exerts on the lipid order of the bilayer.

This kind of discrepancy between the simulated and experimental data is not seen in the case of the DOPC (Ld) bilayer. Similarly, it can be explained by the penetration depth of PRODAN in DOPC bilayers, and its effect on local hydration. When the concentration of PRODAN is increased, the probability that several dye molecules are located in the immediate vicinity of one another is also higher. In this dye aggregate, there could be more water molecules in its local environment as the presence of PRODAN causes the surrounding innermost parts of the bilayer to become more hydrated than the distal parts (Fig 1C). Thus, PRODAN would experience greater dipolar relaxation and a lower sensed GP value.

In addition, the fluorescence lifetime of PRODAN at different concentrations was also investigated (Fig. S4) in vesicles. The Ld phase exhibits a single fluorescence lifetime with a significant ($P < 0.05$, N=5 per concentration) but not a substantial decrease from 3.68 ± 0.03 ns to 3.57 ± 0.03 ns. On the other hand, the Lo phase exhibits two fluorescence lifetimes that both change greatly with increased PRODAN concentration. The first fluorescence lifetime, τ_1, decreases significantly ($P < 0.001$, N = 6 per concentration) from 2.14 ± 0.07 ns at the 1:284 ration to 1.46 ± 0.09 ns at 1:12.5 ratio. On the other hand, the second fluorescence lifetime, τ_2, sees an increase from 5.85 ± 0.02 ns at 1:284 ratio to 6.6 ± 0.3 ns at 1:12.5 ratio ($P < 0.001$, N = 6 for per concentration). Overall, the average fluorescence lifetime of the DPPC:Chol vesicles (Fig. S4 D) shows a significant exponential decrease in the lifetime of the dye ($P < 0.005$, N=6 per concentration) from 3.3 ± 0.1 ns at the lowest concentration to 2.0 ± 0.2 ns at the highest concentration. Similarly, to the GP data, the change in the fluorescence lifetimes of PRODAN in both vesicle types is seen in the same direction even though the hydration and order of lipids changes differently. This data shows that not only does the GP value change with different PRODAN concentrations but other intrinsic properties such as the fluorescence lifetime of the dye also undergo a change. A possible explanation is that when the concentration is increased the dye molecules could aggregate and form excimers or exciplexes.

Interestingly, the same pattern is seen in live cells as for the vesicular data. The GP values of the intracellular Ld phase decreases linearly (Fig. 4D, $P<0.0001$, N=20 for every concentration) from -0.03 ± 0.02 to -0.10 ± 0.02 over a small concentration increase (3.7 - 8.3 μM). A significant ($P<0.0001$, N=20 for every concentration) decrease is also seen in the plasma membrane (Lo phase, Fig. 4C) of the cells. The GP value drops from 0.38 ± 0.03 at the lowest concentration to 0.29 ± 0.03 at the highest concentration. Importantly, the cell membrane is not a pure DPPC:Chol bilayer, it is a very complex environment consisting of dynamic ordered and disordered phases. Whilst cell membranes are a much more complex system than simple single-phase vesicles, the same behaviour is seen in both systems. This suggests that the behaviour observed in pure bilayers could be applied to the cell membrane and be responsible for the apparent decrease in sensed GP of whole cells.

Conclusions

In summary, through the means of MD simulations we have found that the PRODAN affects the local environment of a lipid bilayer differentially depending on the phase of the bilayer. Importantly, we have also investigated its effect on the hydration parameter in different parts of the phospholipid molecules and in different lipid phases. Even though the true lipid order was affected by PRODAN in opposite ways for the two bilayer systems, the experimental data for GUVs and live mammalian cells revealed that this is not reflected in the conventionally used GP value assessment of experimental lipid order. Rather, it depends on the effect that the dye molecules exert on the hydration of the closest regions of the lipid bilayer. We highlight that even a relatively small change in PRODAN concentration can have a significant impact on the sensed GP values in live cells. Although PRODAN is not currently commonly used as an environmentally sensitive dye, its direct derivative Laurdan is popularly used and these findings represent an important advance in understanding how these ES dyes affect their environment, and how their spectroscopic properties relate to the frequently sought lipid bilayers parameters of hydration, lipid order, phase partitioning and molecular mobility. Future investigations involve studying the effect of PRODAN on phospholipids with different headgroups and acyl chains and the effects of different, more complex ES dyes on their local environment. Most importantly, extensions of this research to other ES dyes will be carried out. Indeed, whilst this study shows that PRODAN affects its local environment in a profound way and its use as an ES dye should be interpreted in

Table 1: Average number of water molecules in the first hydration shell of PRODAN's oxygen and nitrogen atoms in the DOPC and DPPC:Chol bilayer

Bilayer	$\langle N_{water} \rangle (oxygen)$	$\langle N_{water} \rangle (nitrogen)$
DOPC	2.20	1.23
DPPC:Chol	2.45	0.47

that context, it is unknown if this effect will be seen in other ES dyes.

Conflicts of interest

There are no conflicts to declare.

Acknowledgements

This work was supported by the Biotechnology and Biological Sciences Research Council [grant number BB/M009513/1] and ERC Starter Grant #337187. We acknowledge the use of the King's College Nikon Imaging Centre (NIC). We are grateful to the UK Materials and Molecular Modelling Hub for computational resources, which is partially funded by EPSRC (EP/P020194/1).

Author Contributions

A.S. performed the simulations, carried out the experiments, analysed the data and wrote the manuscript. A.L.M. helped with fluorescence lifetime imaging. D.J.W helped with cell work. K.S. provided the FLIM microscope. C.L. and D.O. conceived the research.

Notes and references

1 H. E. Grecco, M. Schmick and P. I. H. Bastiaens, *Cell*, 2011, **144**, 897–909.
2 J. K. Lanyi, *J. Biol. Chem.*, 1997, **204**, 18–21.
3 N. M. Hooper and A. J. Turner, *Biochem. J.*, 1988, **250**, 865–869.
4 K. Simons and E. Ikonen, *Nature*, 1997, **387**, 569–72.
5 D. Lingwood and K. Simons, *Science (80-.).*, 2010, **327**, 46–50.
6 K. Simons and M. J. Gerl, *Nat. Rev. Mol. Cell Biol.*, 2010, **11**, 688–699.
7 A. Viola, S. Schroeder, Y. Sakakibara and A. Lanzavecchia, *Science (80-.).*, 1999, **283**, 680–682.
8 K. Akabori, K. Huang, B. W. Treece, M. S. Jablin, B. Maranville, A. Woll, J. F. Nagle, A. E. Garcia and S. Tristram-Nagle, *Biochim. Biophys. Acta - Biomembr.*, 2014, **1838**, 3078–3087.
9 N. Gupta and A. L. DeFranco, *Semin. Cell Dev. Biol.*, 2007, **18**, 616–26.
10 D. M. Owen, C. Rentero, A. Magenau, A. Abu-Siniyeh and K. Gaus, *Nat. Protoc.*, 2012, **7**, 24–35.
11 A. A. Bogdanov and M. L. Mazzanti, *Prog. Mol. Biol. Transl. Sci.*, 2013, **113**, 349–387.
12 E. K. Krasnowska, E. Gratton and T. Parasassi, *Biophys. J.*, 1998, **74**, 1984–1993.
13 B. Mennucci, M. Caricato, F. Ingrosso, C. Cappelli, R. Cammi, J. Tomasi, G. Scalmani and M. J. Frisch, *J. Phys. Chem. B*, 2008, **112**, 414–423.
14 G. Weber and F. J. Farris, *Biochemistry*, 1979, **18**, 3075–3078.
15 T. Parasassi, G. De Stasio, A. D'Ubaldo and E. Gratton, *Biophys. J.*, 1990, **57**, 1179–86.
16 T. Parasassi, G. De Stasio, G. Ravagnan, R. M. Rusch and E. Gratton, *Biophys. J.*, 1991, **60**, 179–189.
17 P. Jurkiewicz, L. Cwiklik, P. Jungwirth and M. Hof, *Biochimie*, 2012, **94**, 26–32.
18 A. Samanta and R. W. Fessenden, *J. Phys. Chem. A*, 2000, **104**, 8972–8975.
19 T. Parasassi, E. K. Krasnowska, L. Bagatolli and E. Gratton, *J. Fluoresc.*, 1998, **8**, 365–373.
20 S. L. Veatch, S. S. W. Leung, R. E. W. Hancock and J. L. Thewalt, *J. Phys. Chem. B*, 2007, **111**, 502–504.
21 H. Bouvrais, T. Pott, L. A. Bagatolli, J. H. Ipsen and P. Méléard, *Biochim. Biophys. Acta - Biomembr.*, 2010, **1798**, 1333–1337.
22 W. K. Nitschke, C. C. Vequi-Suplicy, K. Coutinho and H. Stassen, *J. Phys. Chem. B*, 2012, **116**, 2713–2721.
23 A. L. Obaid, L. M. Loew, J. P. Wuskell and B. M. Salzberg, *J. Neurosci. Methods*, 2004, **134**, 179–190.
24 P. Walde, K. Cosentino, H. Engel and P. Stano, *ChemBioChem*, 2010, **11**, 848–865.
25 A. Marini, A. Muñoz-Losa, A. Biancardi and B. Mennucci, *J. Phys. Chem. B*, 2010, **114**, 17128–35.
26 C. Oostenbrink, A. Villa, A. E. Mark and W. F. Van Gunsteren, *J. Comput. Chem.*, 2004, **25**, 1656–1676.
27 C. Oostenbrink, T. A. Soares, N. F. A. Van Der Vegt and W. F. Van Gunsteren, *Eur. Biophys. J.*, 2005, **34**, 273–284.
28 D. Poger, W. F. Van Gunsteren and A. E. Mark, *J. Comput. Chem.*, 2010, **31**, 1117–1125.
29 H. J. C. Berendsen, J. R. Grigera and T. P. Straatsma, *J. Phys. Chem.*, 1987, **91**, 6269–6271.
30 S. Nosé, *Mol. Phys.*, 1984, **52**, 255–268.
31 M. Parrinello and A. Rahman, *J. Appl. Phys.*, 1981, **52**, 7182–7190.
32 U. Essmann, L. Perera, M. L. Berkowitz, T. Darden, H. Lee and L. G. Pedersen, *J. Chem. Phys.*, 1995, **103**, 8577–8593.
33 B. Hess, *J. Chem. Theory Comput.*, 2008, **4**, 116–122.
34 H. Schindler and J. Seelig, *Biochemistry*, 1975, **14**, 2283–2287.